Letter

Observation of electronic structure and electron-boson coupling in the low-dimensional superconductor $Ta_4Pd_3Te_{16}$

H. F. Yang,[1,*] X. L. Liu,[1,*] S. M. Nie,[2] W. J. Shi,[3] K. Huang,[1] H. J. Zheng,[1] J. Zhang,[1] Y. W. Li,[1] A. J. Liang,[1,4] M. X. Wang,[1,4] L. X. Yang,[5] Y. F. Guo,[1,†] Z. K. Liu,[1,4,‡] and Y. L. Chen[1,4,5,6,§]

[1]*School of Physical Science and Technology, ShanghaiTech University, Shanghai 201210, China*
[2]*Department of Materials Science and Engineering, Stanford University, Stanford, California 94305, USA*
[3]*Center for Transformative Science, Shanghai High Repetition Rate XFEL and Extreme Light Facility (SHINE), ShanghaiTech University, Shanghai 201210, China*
[4]*ShanghaiTech Laboratory for Topological Physics, 201210 Shanghai, China*
[5]*State Key Laboratory of Low Dimensional Quantum Physics and Department of Physics, Tsinghua University, Beijing 100084, China*
[6]*Department of Physics, University of Oxford, Oxford, OX1 3PU, United Kingdom*

(Received 25 May 2021; revised 14 September 2021; accepted 12 November 2021; published 1 December 2021)

Ternary telluride $Ta_4Pd_3Te_{16}$ is a layered superconductor with quasi-one-dimensional characteristics. It has attracted great research interests due to the possible nodal superconductivity and its interplay with adjacent charge-density wave as well as proposed nontrivial band topology. Here, we report low-energy electronic band structure of $Ta_4Pd_3Te_{16}$ by means of high-resolution laser-based angle-resolved photoemission spectroscopy. We acquired the Fermi surface and detailed band dispersions, directly reflecting its multiband nature. Furthermore, dispersion kinks at ∼8 meV below the Fermi level are unambiguously observed, indicative of strong electron-boson coupling. We suggest these kinks are probably due to electron-phonon coupling with effective coupling constants quantified to be ∼0.72 and ∼0.48 for the γ_1 and γ_2 bands, respectively. Our results provide valuable information for future studies on the mechanism of superconductivity as well as its intimacy to charge-density wave in $Ta_4Pd_3Te_{16}$.

DOI: 10.1103/PhysRevB.104.L220501

Discovering new superconductors and investigating their superconducting mechanism is one of the most significant themes in condensed-matter physics [1–3]. Ternary telluride $Ta_4Pd_3Te_{16}$ is discovered to exhibit superconductivity at ∼4.6 K [4] that is further enhanced to 6.7 K at a pressure of 3.1 kPa [5]. It has stimulated great research interests, due to its mixed dimensions in its crystal structure [4], possible unconventional superconductivity [5–8] coexisting with charge-density wave (CDW) orders [9–11], and proposed nontrivial band topology [12].

$Ta_4Pd_3Te_{16}$ crystallizes in a layered structure and each two-dimensional plane consists of one-dimensional chains, thus exhibiting strong quasi-one-dimensional characteristics [4] that further could lead to the appearance of density waves and even enhanced electronic correlations. Heated debate on whether its superconductivity is unconventional is ongoing [5–9,13,14]. Thermal conductivity measurements claimed the nodes in the superconducting gaps, based on significant residual linear term of thermal conductivity in zero magnetic field and its strong field dependence [5]. Gap node within a multiband scenario was also suggested by specific-heat analysis [6], London penetration depth measurements [7], and scanning tunneling microscope (STM) studies [8], as their experimental data can be nicely fitted by respective formulas with gap nodes. By contrast, nuclear magnetic/quadrupole resonance (NMR/NQR) studies reported a Hebel-Slichter coherence peak just below T_C (superconducting transition temperature) for ^{125}Te, and characterize it as an *s*-wave nodeless superconductor [9], which is in line with another STM study [13].

In close proximity to superconductivity lies the CDW phase. A CDW order in $Ta_4Pd_3Te_{16}$ was reported to set in around 20 K by NMR/NQR [9] and transport measurements [10]. Very recently, the synchrotron x-ray diffraction further revealed the CDW order to be a two-dimensional incommensurate one with wave vectors $Q_1 = [-0.2, 0.21, -0.3]$ and $Q_2 = [0.2, 0.21, 0.3]$ [11]. The CDW transition or fluctuation was also suggested at high temperatures (140 to 200 K) below which the linewidth of one A_g phonon mode at 89.9 cm^{-1} shows an unconventional increase in Raman scattering measurements [15]. However, the CDW transition is not accompanied by the Fermi surface reconstruction according to the de Haas–van Alphen quantum oscillation measurements [10,11]. In addition, high-throughput calculation analysis suggests nontrivial band topology in $Ta_4Pd_3Te_{16}$ [12], rendering it a topological superconductor candidate [16,17].

All these render $Ta_4Pd_3Te_{16}$ an interesting material system with rich physics that merits further studies. One important milestone is measuring momentum-resolved electronic structure that could provide valuable information for deepening the understanding on this system in regard to the

*These authors contributed equally to this work.
†guoyf@shanghaitech.edu.cn
‡liuzhk@shanghaitech.edu.cn
§yulin.chen@physics.ox.ac.uk

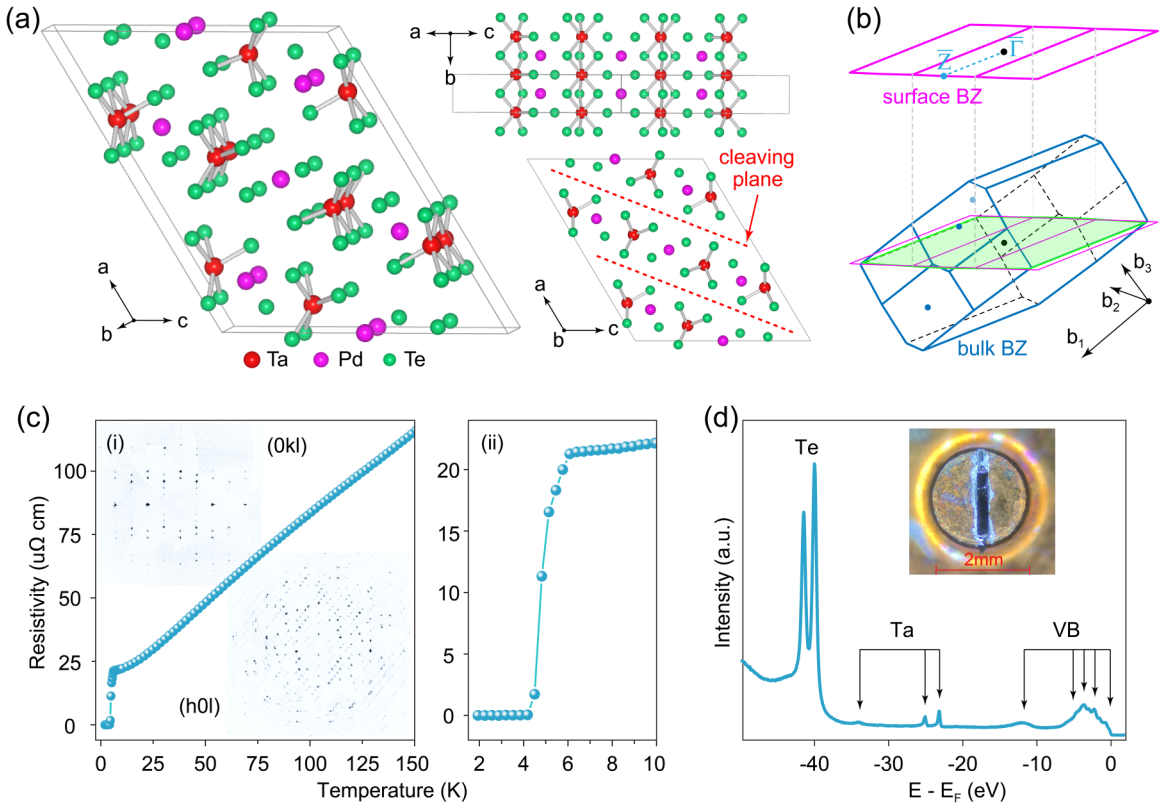

FIG. 1. (a) Crystal structure of $Ta_4Pd_3Te_{16}$ viewed from three different directions. Dotted red line represents the cleaving plane –(2 0 1) in the conventional cell. (b) Bulk and surface Brillouin zones (BZs). The ARPES measurement plane corresponding to the (2 0 1) cleaving plane is parallel to the green shade marked in bulk BZ (note that the ARPES measurement plane should be a slightly curved plane). b_1, b_2, and b_3 mark directions of reciprocal lattice vectors. (c) Large-scale (i) and zoomed-in plot (ii) of temperature dependence of electrical resistivity of $Ta_4Pd_3Te_{16}$. The inset of (i) displays x-ray diffraction patterns on crystals. (d) Photoemission core-level measurements (core levels of Pd are outside of the energy range). The inset is the optical image of the cleaved crystal.

superconducting mechanism, CDW ordering, and potential nontrivial band topology. Unfortunately, this study has not been reported so far.

Here, we report high-resolution laser-based angle-resolved photoemission spectroscopy (ARPES) measurements on $Ta_4Pd_3Te_{16}$ crystals. We acquire the Fermi surface and detailed band dispersion of the normal state, directly reflecting its multiband nature. Moreover, we unambiguously observe dispersion kinks at ~8 meV below the Fermi level (E_F), evidencing strong electron-boson coupling. We argue that these kinks are probably due to the electron-phonon coupling with the effective coupling constant (λ_{eff}) estimated to be ~0.72 and ~0.48 for γ_1 and γ_2 bands, respectively.

$Ta_4Pd_3Te_{16}$ crystallize in a base-centered monoclinic structure with the space group of $C2/m$ (No. 12) and lattice parameters of $a = 21.276$ Å, $b = 3.735$ Å, $c = 17.687$ Å, $\beta = 120.75°$. As shown in Fig. 1(a), it exhibits a layered structure with inversion and mirror symmetries (with respect to ac plane), and each layer is constituted of one-dimensional chains of PTe_2, Ta_2Te_4, and $TaTe_3$, thus showing mixed dimensions. $Ta_4Pd_3Te_{16}$ is gifted with a natural cleaving plane, the (2 0 1) plane within the conventional cell we choose, and corresponding measurement plane of ARPES is parallel to the green shade in three-dimensional bulk Brillouin zone (BZ) in Fig. 1(b). Surface BZ (in magenta) and relevant high-symmetry points are adopted for the convenience of describing the ARPES data. High-quality $Ta_4Pd_3Te_{16}$ crystals synthesized by the self-flux method [4], exhibit sharp x-ray diffraction patterns [insets of Fig. 1(c)] as well as sharp core-level peaks in photoemission core-level measurements [Fig. 1(d)]. Electrical resistivity measurements confirm the superconducting transition occurs at ~4.8 K [Fig. 1(c)], in line with previous reports [4]. Crystals are *in situ* cleaved at 40 K for laser-ARPES measurements (6.994 eV) with laser beam size smaller than 30 um (as crystals are soft and narrow, ARPES with focused laser beam is highly desirable to get rid of multidomain effects to acquire reliable data). The overall momentum and energy resolutions are 0.003 $Å^{-1}$ and 3 meV, respectively; the base pressure of the ARPES chamber is better than 3×10^{-11} mbar.

Figure 2 displays measured band structure of $Ta_4Pd_3Te_{16}$ in the normal state. The Fermi surface consists of multiple sheets stretching along the k_x axis and expanding dramatically to cover almost the whole momentum space upon increasing the binding energy. It shows a nice resemblance to the published calculations of Fermi surface [10,14] (Fig. S1 of Supplemental Material [18]; see also Refs. [19,20] therein), which allows us to qualitatively assign bands as α, β, γ, and δ for simply describing the band structure [Fig. 2a(i)]. While α and δ are blurry, the β and γ are sharp and show strong quasi-one-dimensional nature according to the calculations [14]. The band dispersion cut along the $\bar{\Gamma} - \bar{Z}$ direction shows

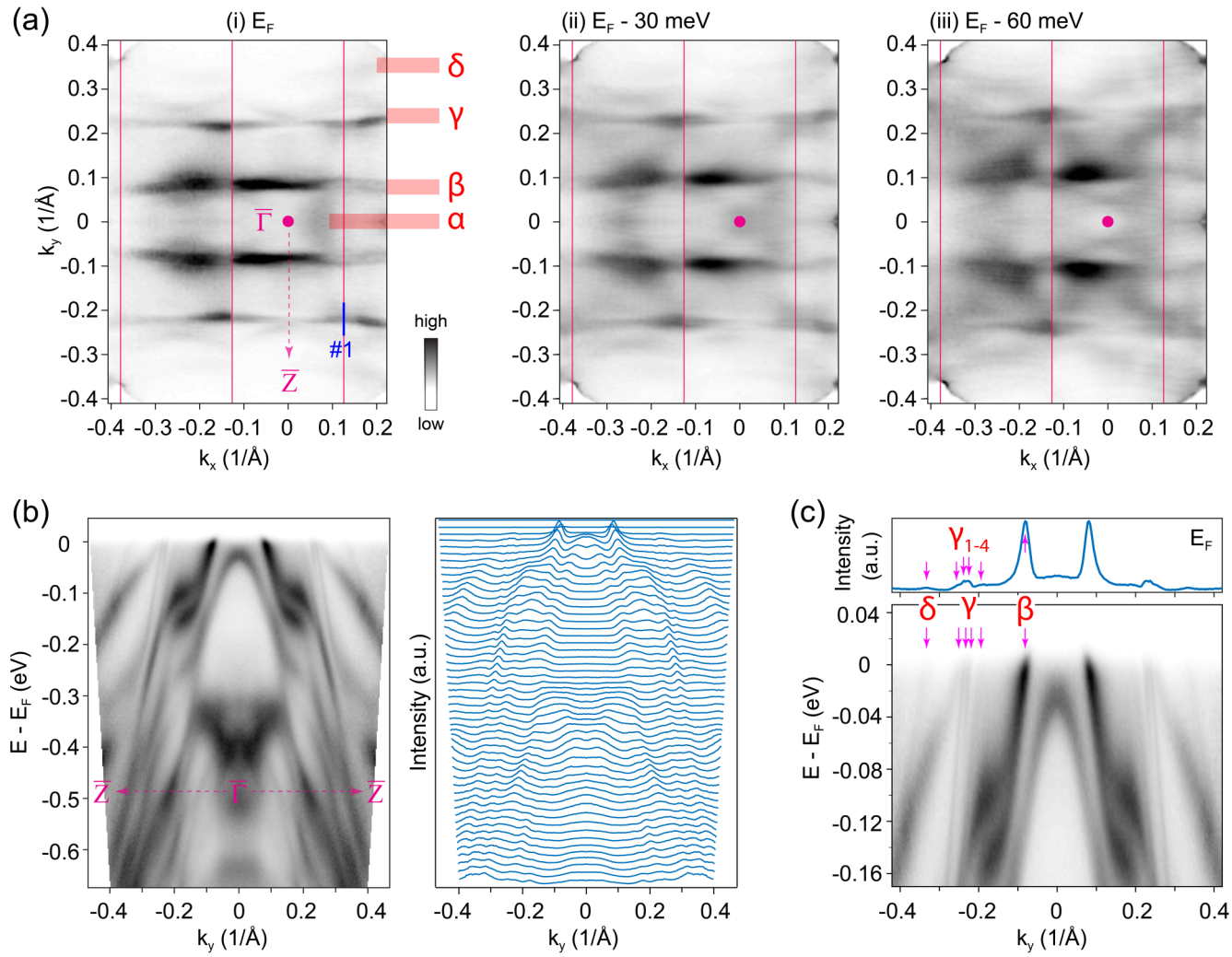

FIG. 2. (a) Constant energy contours of $Ta_4Pd_3Te_{16}$ at E_F (i), E_F–30 meV (ii), E_F–60 meV (iii), measured with 6.994-eV laser at 30 K. The integration window is [E_B–5 meV, E_B + 5 meV]. Overlaid magenta curves are the surface BZ that we adopt for simplicity to describe band structures. The photoemission spectra are mirrored with respect to $k_y = 0$ according to the mirror symmetry of crystals. The measured Fermi surface (i) shows a nice resemblance to the published calculations of bulk Fermi surface (Fig. S1 of Supplemental Material [18]), allowing us to qualitatively assign bands as α, β, γ, and δ for simply describing the band structure. (b) The photoemission intensity spectrum (left panel) and its MDC plot (right panel) along the $\bar{\Gamma} - \bar{Z}$ direction. (c) Near-E_F zoom-in photoemission intensity spectrum (lower panel) and the MDC at E_F (upper panel), clearly showing six discernible band crossings. Near-E_F band structures are dominated by Te ($5p_x$, $5p_y$, and $5p_z$ orbitals) with small contributions from Ta ($5d_{x2}$ and $5d_{xz}$ orbitals) and Pd ($4d_{z2}$ orbital) (Figs. S4 and S5 in Supplemental Material [18]).

six discernible band crossings, four of which are assigned to the γ (further labeled as γ_1, γ_2, γ_3, γ_4), as shown in Figs. 2(b) and 2(c). We cannot rule out the possibility of the existence of surface states in these six bands, and these potential surface states are topological trivial as our detailed Wilson loop calculations show $Ta_4Pd_3Te_{16}$ is actually trivial with the topological invariant $Z_2 = 0$ (Fig. S2 of Supplemental Material [18]).

Interestingly, we observe dispersion kinks near E_F, indicating strong electron-boson coupling. Figure 3a(i) displays the measured photoemission intensity as functions of momentum and binding energy along #1 [marked in Fig. 2a(i)], in which γ_1 and γ_2 bands are clearly shown. Apparently, a dispersion kink appears at 8 meV below E_F for both γ_1 and γ_2 bands, as marked by magenta and cyan arrows. These dispersion kinks are further revealed by dividing the raw data [Fig. 3a(i)] with the Fermi-Dirac distribution function [Fig. 3a(ii)], stacked momentum distribution curve (MDC) plots [Fig. 3a(iii)], and quantitatively extracted dispersions of γ_1 and γ_2 bands by fitting these MDCs [Fig. 3(b)]. Further, we carry out the electron self-energy analysis which is commonly done in studying dispersion kinks of many correlated systems like cuprates [3,21]. The effective real part of the self-energy ($\mathrm{Re}\Sigma$) is extracted from dispersions by assuming a straight line as the featureless empirical bare band [dotted cyan lines in Fig. 3(b)]. As shown in Fig. 3(c), $\mathrm{Re}\Sigma$ exhibits a prominent peak at 8 ± 1 meV for both γ_1 and γ_2 bands. This is qualitatively consistent with the increase of MDC peak width (related to the imaginary part of the self-energy and inversely proportional to the quasiparticle lifetime), again confirming the existence of dispersion kinks at ~8 meV. (We note that the slight misalignment of $\mathrm{Re}\Sigma$ peak and the slope midpoint in MDC peak width is probably due to

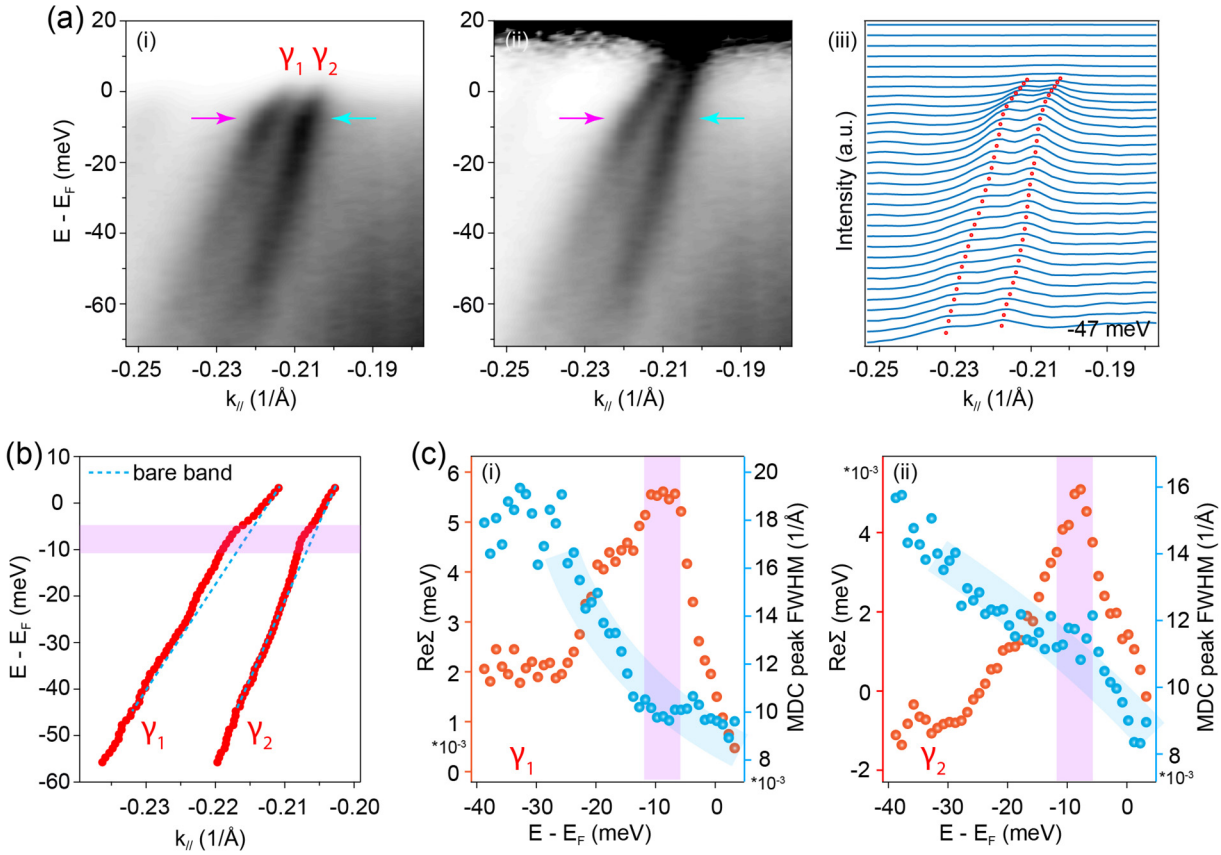

FIG. 3. (a) Photoemission intensity spectrum along #1 [marked in Fig. 2a(i)] (i), that is further divided by the Fermi-Dirac distribution function with the temperature of 30 K (ii). (iii) is the related MDC plot (E_B ranges from 14 to −47 meV) in which red balls tracing the band dispersion are a guide to the eye. [Note that this dispersion and that in Fig. 2(c) are from different momentum directions and locations.] Dispersion kinks at 8 meV below E_F are apparently observed, as marked by magenta and cyan arrows. (b) Extracted dispersions of γ_1 and γ_2 by MDC peak fitting with two Lorentzian peaks plus a linear background. Dotted cyan lines are empirical bare bands we choose for self-energy analysis. Magenta shadow marks the kink region. (c) Real part of the self-energy and MDC peak (full width at half maxima) of γ_1 and γ_2 bands. Magenta shadows mark the kink. The real part features a peak at the kink energy, while MDC peak width exhibits an abrupt change.

fitting uncertainties.) No kinks are confidently confirmed on β- and δ bands (Fig. S6 of Supplemental Material [18]).

In principle, a kink in the dispersion is the hallmark of strong electron-boson coupling and the kink marks the energy of the bosonic mode [21]. It is observed in many correlated systems [22–27], and one famous example is the cuprate of which the kink origin is believed to be intimately related to the mechanism of high-temperature unconventional superconductivity [3]. What is the origin of dispersion kinks in $Ta_4Pd_3Te_{16}$? The electron-phonon coupling serves as a feasible explanation [3,28]. Previous polarized Raman scattering studies suggest strong electron-phonon coupling, as they discover the linewidth of one A_g phonon mode at 89.9 cm^{-1} (∼11.1 meV) increases unconventionally with decreasing temperature [15] (we note that Raman linewidth broadening is not directly related to electron-phonon coupling; in addition to electron-phonon interactions, lattice anharmonicity can also give rise to anomalous phonon linewidth evolution). The energy scale of this phonon mode is close to the binding energy of the kink we observed (other candidate modes include the A_g mode at 65.7 cm^{-1} and the B_g mode at 89.1 cm^{-1} [15] as their energies are also close to the kink energy from ARPES measurements). The existence of CDW order also suggests the strong coupling between electrons and phonons, as CDW is always accompanied with lattice distortions. Further, we can quantify the effective coupling constant (λ_{eff}) by taking the ratio between the high binding-energy velocity above the kink energy and the "dressed" velocity below the kink energy (which is $1 + \lambda_{eff}$) [21]. The λ_{eff} values for γ_1 and γ_2 are ∼0.72 and ∼0.48, respectively, (which are close to 0.77–the electron-phonon coupling constant calculated via McMillan formula [4]). Note that our λ_{eff} is slightly underestimated as we underestimate the bare velocity by involving the electron-electron correlation (directly manifested by T^2 dependence of resistivity [4,29,30] and large Wilson ratio [31]). On the other hand, electron-magnon coupling cannot be completely excluded. Although $Ta_4Pd_3Te_{16}$ does not possess long-range magnetic ordering and is located far away from magnetic instability due to the weak contribution of d electrons of Ta and Pd to the Fermi surface [14], the spin fluctuations cannot be precluded if moments exist which however need further verification. The origin of the dispersion kink deserves further scrutiny while our data may serve as a concrete starting point.

The general band structure and low-energy dispersion kinks acquired by ARPES can highly benefit studies on the

mixed dimensionality, band topology, CDW, and superconductivity in $Ta_4Pd_3Te_{16}$. The Fermi surface we measured directly confirmed the mixed dimensionality. Especially, sharp β- and γ bands exhibit quasi-one-dimensional nature, and are parallel to each other. This may raise instability that accounts for the CDW that needs further investigations. No signatures of Luttinger liquid behaviors on β-and γ bands are observed. Multiband nature should be taken into account in interpreting experimental data towards the superconducting mechanisms, and electron-phonon coupling should be considered. In addition, the trivial band topology rules out the possibility of $Ta_4Pd_3Te_{16}$ as a topological superconductor candidate.

In summary, we directly measured multiband structures of $Ta_4P_3Te_{16}$ via laser-AREPS with high resolutions. Strong electron-boson coupling is directly revealed by evident dispersion kinks at ~8 meV below E_F. This is most probably due to electron-phonon coupling. While future studies are highly desirable to finally pin down the superconducting pairing symmetry as well as its interplay with adjacent CDW, our results can provide a valuable starting point.

We wish to thank D. J. Singh for insightful discussions. This work is sponsored by Shanghai Sailing Program (Grant No. 20YF1430500 to H.F.Y.), the National Natural Science Foundation of China (Grant No. 12004248 to H.F.Y., Grant No. 92065201 to Y.F.G., Grants No. 11634009 and No. 11674229 to Y.L.C. and Z.K.L.), the Shanghai Municipal Science and Technology Major Project (Grant No. 2018SHZDZX02 to Y.L.C. and Z.K.L.), the National Key R&D Program of China (Grant No. 2017YFA0305400 to Z.K.L.). We acknowledge ARPES beamlines for preliminary ARPES measurements: BL03U of Shanghai Synchrotron Radiation Facility, and BL13U of National Synchrotron Radiation Laboratory, SpectroMicroscopy (nano-ARPES) in Elettra. We also acknowledge the Analytical Instrumentation Center of ShanghaiTech University for x-ray and Laue diffraction measurements.

[1] P. A. Lee, N. Nagaosa, and X.-G. Wen, Rev. Mod. Phys. **78**, 17 (2006).
[2] G. R. Stewart, Rev. Mod. Phys. **83**, 1589 (2011).
[3] A. Damascelli, Z. Hussain, and Z.-X. Shen, Rev. Mod. Phys. **75**, 473 (2003).
[4] W. H. Jiao, Z. T. Tang, Y. L. Sun, Y. Liu, Q. Tao, C. M. Feng, Y. W. Zeng, Z. A. Xu, and G. H. Cao, J. Am. Chem. Soc. **136**, 1284 (2014).
[5] J. Pan, W. H. Jiao, X. C. Hong, Z. Zhang, L. P. He, P. L. Cai, J. Zhang, G. H. Cao, and S. Y. Li, Phys. Rev. B **92**, 180505(R) (2015).
[6] W.-H. Jiao, Y. Liu, Y.-K. Li, X.-F. Xu, J.-K. Bao, C.-M. Feng, S. Y. Li, Z.-A. Xu, and G.-H. Cao, J. Phys.: Condens. Matter **27**, 325701 (2015).
[7] G. Pang, M. Smidman, W. Jiao, L. Jiao, Z. Weng, W. Jiang, C. Guo, Y. Chen, G. Cao, and H. Yuan, J. Phys.: Condens. Matter **30**, 055701 (2018).
[8] Z. Du, D. Fang, Z. Wang, Y. Li, G. Du, H. Yang, X. Zhu, and H. H. Wen, Sci. Rep. **5**, 9408 (2015).
[9] Z. Li, W. H. Jiao, G. H. Cao, and G.-Q. Zheng, Phys. Rev. B **94**, 174511 (2016).
[10] T. Helm, F. Flicker, R. Kealhofer, P. J. W. Moll, I. M. Hayes, N. P. Breznay, Z. Li, S. G. Louie, Q. R. Zhang, L. Balicas, J. E. Moore, and J. G. Analytis, Phys. Rev. B **95**, 075121 (2017).
[11] Z. Shi, S. J. Kuhn, F. Flicker, T. Helm, J. Lee, W. Steinhardt, S. Dissanayake, D. Graf, J. Ruff, G. Fabbris, D. Haskel, and S. Haravifard, Phys. Rev. Res. **2**, 042042 (R) (2020).
[12] T. Zhang, Y. Jiang, Z. Song, H. Huang, Y. He, Z. Fang, H. Weng, and C. Fang, Nature (London) **566**, 475 (2019).
[13] Q. Fan, W. H. Zhang, X. Liu, Y. J. Yan, M. Q. Ren, M. Xia, H. Y. Chen, D. F. Xu, Z. R. Ye, W. H. Jiao, G. H. Cao, B. P. Xie, T. Zhang, and D. L. Feng, Phys. Rev. B **91**, 104506 (2015).
[14] D. J. Singh, Phys. Rev. B **90**, 144501 (2014).
[15] D. Chen, P. Richard, Z. D. Song, W. L. Zhang, S. F. Wu, W. H. Jiao, Z. Fang, G. H. Cao, and H. Ding, J. Phys.: Condens. Matter **27**, 495701 (2015).
[16] X.-L. Qi and S.-C. Zhang, Rev. Mod. Phys. **83**, 1057 (2011).
[17] P. Zhang, K. Yaji, T. Hashimoto, Y. Ota, T. Kondo, K. Okazaki, Z. Wang, J. Wen, G. D. Gu, H. Ding, and S. Shin, Science **360**, 182 (2018).
[18] See Supplemental Material at http://link.aps.org/supplemental/10.1103/PhysRevB.104.L220501 for details on methods of sample growth and ARPES measurements, comparison of measured and calculated Fermi surface in 3D BZ, detailed calculations showing $Ta_4Pd_3Te_{16}$ is topologically trivial, estimation of effective coupling constants, element and orbital contributions to near-EF band structures, and discussions on the fact that no kinks are confidently confirmed on β - and δ bands.
[19] G. Kresse and J. Furthmüller, Phys. Rev. B **54**, 11169 (1996).
[20] J. P. Perdew, K. Burke, and M. Ernzerhof, Phys. Rev. Lett. **77**, 3865 (1996).
[21] A. Lanzara, P. V. Bogdanov, X. J. Zhou, S. A. Kellar, D. L. Feng, E. D. Lu, T. Yoshida, H. Eisaki, A. Fujimori, K. Kishio, J.-I. Shimoyama, T. Noda, S. Uchida, Z. Hussain, and Z.-X. Shen, Nature (London) **412**, 510 (2001).
[22] C. Li, G. Dai, Y. Cai, Y. Wang, X. Wang, Q. Gao, G. Liu, Y. Huang, Q. Wang, F. Zhang, S. Zhang, F. Yang, Z. Wang, Q. Peng, Z. Xu, C. Jin, L. Zhao, and X. J. Zhou, Chin. Phys. B **29**, 107402 (2020).
[23] Y. Hu, X. Chen, S. T. Peng, C. Lane, M. Matzelle, Z. L. Sun, M. Hashimoto, D. H. Lu, E. F. Schwier, M. Arita, T. Wu, R. S. Markiewicz, K. Shimada, X. H. Chen, Z. X. Shen, A. Bansil, S. D. Wilson, and J. F. He, Phys. Rev. Lett. **123**, 216402 (2019).
[24] H. F. Yang, Z. T. Liu, C. C. Fan, Q. Yao, P. Xiang, K. L. Zhang, M. Y. Li, H. Li, J. S. Liu, D. W. Shen, and M. H. Jiang, Phys. Rev. B. **93**. 121102 (2016).
[25] D. E. Shai, C. Adamo, D. W. Shen, C. M. Brooks, J. W. Harter, E. J. Monkman, B. Burganov, D. G. Schlom, and K. M. Shen, Phys. Rev. Lett. **110**, 087004 (2013).
[26] Z. Sun, Y. D. Chuang, A. V. Fedorov, J. F. Douglas, D. Reznik, F. Weber, N. Aliouane, D. N. Argyriou, H. Zheng, J. F. Mitchell,

T. Kimura, Y. Tokura, A. Revcolevschi, and D. S. Dessau, Phys. Rev. Lett. **97**, 056401 (2006).

[27] S. Aizaki, T. Yoshida, K. Yoshimatsu, M. Takizawa, M. Minohara, S. Ideta, A. Fujimori, K. Gupta, P. Mahadevan, K. Horiba, H. Kumigashira, and M. Oshima, Phys. Rev. Lett. **109**, 056401 (2012).

[28] F. Giustino, Rev. Mod. Phys. **89**, 015003 (2017).

[29] R. Goyal, B. Tiwari, R. Jha, and V. P. S. Awana, J. Supercond. Novel Magn. **28**, 1195 (2015).

[30] Q. R. Zhang, D. Rhodes, B. Zeng, M. D. Johannes, and L. Balicas, Phys. Rev. B **94**, 094511 (2016).

[31] W. H. Jiao, Y. N. Huang, X. F. Xu, Y. K. Li, Y. Liu, Z. C. Wang, X. L. Xu, Y. X. Feng, C. M. Feng, and G. H. Cao, J. Phys.: Condens. Matter **31**, 325601 (2019).